Comparison of ground-structure and continuum based topology optimization methods for strut-and-tie model generation

Xia, Yi; Liew, Andrew; Wu, Hongfei; Langelaar, Matthijs; Hendriks, Max A.N.; Yang, Yuanlong; Takalloozadeh, Meisam; Gilbert, Matthew

DOI
10.1016/j.engstruct.2024.118498

Publication date
2024

Document Version
Final published version

Published in
Engineering Structures

Citation (APA)
Xia, Y., Liew, A., Wu, H., Langelaar, M., Hendriks, M. A. N., Yang, Y., Takalloozadeh, M., & Gilbert, M. (2024). Comparison of ground-structure and continuum based topology optimization methods for strut-and-tie model generation. *Engineering Structures*, *316*, Article 118498. https://doi.org/10.1016/j.engstruct.2024.118498

Engineering Structures 316 (2024) 118498

Contents lists available at ScienceDirect

Engineering Structures

journal homepage: www.elsevier.com/locate/engstruct

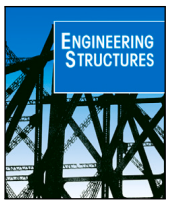

Comparison of ground-structure and continuum based topology optimization methods for strut-and-tie model generation

Yi Xia [a,b], Andrew Liew [c], Hongfei Wu [a,b], Matthijs Langelaar [d], Max A.N. Hendriks [e,f], Yuanlong Yang [a,b], Meisam Takalloozadeh [g,h], Matthew Gilbert [g,*]

[a] School of Civil Engineering, Chongqing University, Chongqing, 400045, China
[b] Key Laboratory of New Technology for Construction of Cities in Mountain Area of Ministry of Education, Chongqing University, Chongqing, 400045, China
[c] Unipart Construction Technologies Ltd, Sheffield, UK
[d] Faculty of Mechanical Engineering, Delft University of Technology, Delft, Netherlands
[e] Faculty of Civil Engineering & Geosciences, Delft University of Technology, Delft, Netherlands
[f] Department of Structural Engineering, Norwegian University of Science and Technology (NTNU), Trondheim, Norway
[g] Department of Civil and Structural Engineering, The University of Sheffield, Sheffield, UK
[h] Department of Civil and Environmental Engineering, School of Engineering, Shiraz University, Shiraz, Iran

ARTICLE INFO

Keywords:
Reinforced concrete
Strut-and-tie
Truss topology optimization
Continuum topology optimization
Ground-structure method
Layout optimization

ABSTRACT

When employing the strut-and-tie modelling (STM) method in the conceptual design of reinforced concrete structures, a suitable strut-and-tie (ST) model indicating load transfer mechanisms first needs to be identified. Topology optimization (TO) methods have frequently been used for this purpose. However, although TO methods employing either a ground-structure or a continuum-based TO approach can be used, the performance and effectiveness of these two methods have not been systematically investigated and compared. To obtain a better understanding of the characteristics of both methods, a systematic comparison procedure is proposed to investigate the generation process and the resulting ST designs. Three aspects, relating to structural performance, economic issues, and method applicability are considered in the comparison, with six metrics formulated to quantify these aspects. Based on investigation of designs for three reinforced concrete elements incorporating typical discontinuity regions (two 2D cases and a 3D case), the performance of the two methods is assessed. It is found that both methods result in safe and efficient ST designs, with comparable structural performance, while some differences in terms of computation time and usability are observed.

1. Introduction

In the conceptual design of reinforced concrete structures, the strut-and-tie modelling (STM) method plays an important role, especially for structures with discontinuity regions (D-regions). Compared to standard Bernoulli regions (B-regions), where a linear strain distribution is observed, a highly nonlinear strain distribution appears in D-regions. This nonlinear strain distribution makes it difficult for engineers to obtain safe and economical designs. The STM method was initially proposed by Ritter [1] and Mörsch [2] over a century ago, and was generalized by Schlaich and Schafer [3] and Schlaich et al. [4] as a consistent design method for reinforced concrete structures. The STM method uses a truss system, known as a strut-and-tie (ST) model, to indicate the complex force transfer mechanisms in a D-region. The STM method takes advantage of the lower-bound theory of plasticity [5,6], with axial force equilibrium required but strain compatibility ignored [7]. The STM method provides a simple and effective design approach for practical application, and is referred to in many current design codes, e.g., CEN [8], fib [9], ACI [10], CSA [11] and AASHTO [12] codes.

Since complex reinforced concrete structures are now frequently approximated using ST models, it is important that effective means of identifying such models are available. However, according to lower-bound plasticity theory, there are generally multiple possible ST models for the same design problem, and it can be a challenging task for engineers to find a suitable truss system when applying the STM method. Traditionally, ST models for analysing D-regions were selected based on an engineer's experience [13–15]. However, this process includes subjective aspects and relies heavily on the experience of the engineer involved. Also, when a design problem becomes complex, for example involving an irregular geometry and/or multiple loading conditions, finding a suitable ST model may be beyond the capability of many

* Corresponding author.
E-mail address: m.gilbert@sheffield.ac.uk (M. Gilbert).

https://doi.org/10.1016/j.engstruct.2024.118498
Received 7 January 2024; Received in revised form 5 June 2024; Accepted 22 June 2024
Available online 14 July 2024

engineers. A recent investigation [16] indicates that the calculated resistance of an RC half-joint is affected by which STM bars are active. In order to address this problem, topology optimization (TO) methods have been proposed to generate ST models.

TO methods have been investigated by many workers and are powerful tools for a range of structural design applications. Such methods provide a systematic means of identifying optimized material distributions based on given loading and support conditions. The resulting material distributions can indicate the load paths within the investigated structure. Two categories of TO methods have been used for the STM investigations. Firstly, the ground-structure-based topology optimization (GS-TO) method [17], also frequently referred to as 'truss topology optimization' or 'truss layout optimization', has been applied. In the GS-TO method, the region under consideration is discretized using nodes that are then interconnected with truss bars to form a so-called 'ground-structure'. During the optimization process the subset of truss bars forming the optimal structure is identified. GS-TO methods appear to have been first adopted for the generation of ST models in [18–21], though Kwak and Noh [22] subsequently proposed an evolutionary structural optimization method based on brick elements (repetitive assemblies of truss elements) for STM. Similarly, Zhong et al. [23,24] proposed a micro-truss-based TO method for generating ST models. A highly efficient means of identifying trusses to inform ST models was proposed by Bołbotowski and Sokół [25]. However, relatively complex ST models, with numerous members, were often obtained in these studies.

Compared to the GS-TO methods, another approach is to use continuum-based topology optimization (C-TO) methods for ST model generation. In this category, evolutionary structural optimization (ESO) methods have been used to obtain optimized material layouts for creating ST models [26–29]. In addition, the application of other TO methods for STM has also been extensively investigated, such as SIMP (solid isotropic material with penalization) methods [30–33], BESO (Bi-directional ESO) methods [34,35] and a homogenization optimization method [36]. The integration of GS-TO and C-TO methods has also been investigated [37,38], where tensile members and compressive regions were represented by ground-structures and continuum respectively.

Whichever approach is used, TO methods provide a systematic means of indicating load transfer mechanisms, which can then be used to develop ST models. This reduces manual effort and the level of experience required by an engineer seeking a suitable ST model. In addition to TO based methods, various other systematic methods have also been proposed for STM model generation. For example, load path approaches, in which the configuration of ST models is determined through either the force path or the stress field obtained from finite element analysis, have been proposed [39–41].

Although various investigations involving applying different TO methods to STM have been conducted, the relative performance of GS-TO and C-TO methods has to date not been systematically investigated and compared. Compared to ground-structure-based strut-and-tie models (GS-STMs), in the case of continuum-based strut-and-tie models (C-STMs), the optimized continuum material layouts generated cannot be directly used as truss-analogy models for STM [42]. In this case a manual process is required to transform an optimized continuum to a ST model. This issue makes it difficult to systematically compare the two methods, although a method to generate C-STMs automatically was recently proposed [43,44]. On the other hand, as already mentioned, a challenge associated with using GS-STM methods is to produce ST models that are sufficiently simple and practical. To seek to address this geometry optimization and/or the use of joint costs to penalize short members can be applied [45], as will be employed in the present study, though more powerful means of simplifying results have also recently been proposed in [46,47]. A recent experimental study involving reinforced concrete girders in which STM designs were compared with those based on European design codes showed that the former had higher load-carrying capacities and lower material usage [48]. In addition, the effectiveness and applicability of GS-based optimization methods when additive manufacturing processes are employed were presented in [49]. These developments, i.e. automatic truss extraction for C-ST and simplification methods for GS-ST models, enable wider application of TO-based STM methods, and also provide a basis for a systematic comparison of the two approaches.

In this paper, to investigate the performance of the two types of STM generation methods, the GS-STM generation method based on [45] and the C-STM generation method based on [43,44,50] are investigated. A systematic comparison procedure is proposed, considering three main aspects: structural performance, economic benefits and method applicability. To quantify these aspects when comparing the two STM generation methods, six metrics are formulated, based on the generated ST models and resulting designs. For several typical 2D/3D D-regions, the corresponding GS-STMs and C-STMs are generated and the resulting STM designs are analysed. In addition, TO input parameters that affect ST model generation are investigated, with the generated STMs also evaluated and compared. This appears to be the first study to systematically evaluate the two main categories of STM generation method. The aim of the work is to gain a better understanding of the strengths and weaknesses of the two approaches, and to identify areas for future research. Note that due to the large numbers of designs generated in the present study, here non-linear finite element analysis (NLFEA) [43,44,50] is used to compare structural performance, considering cracking and crushing of the concrete and yielding and fracturing of the steel; extending the study to encompass experimental investigation is therefore a topic for future research.

The paper is organized as follows: details of the GS-STM and C-STM generation methods are briefly introduced in Section 2, with key differences between the two methods also discussed. In Section 3, six metrics for evaluating the two methods are formulated and a comparison procedure is proposed. In Section 4, three typical D-regions (a deep beam with an opening, a 2D voided beam and a 3D voided slab) are investigated. The corresponding GS-STMs and C-STMs are generated and analysed based on the proposed comparison procedure. Through a comprehensive evaluation of a range of ST models, the influence of the parameters used by the two methods is discussed in Section 5. Finally, conclusions are drawn and possible future investigations are summarized in Section 6.

2. Strut-and-tie model generation based on two topology optimization methods

In this section, details of the two methods of ST model generation, shown diagrammatically in Fig. 1, are introduced; key differences between these methods are then highlighted.

2.1. Ground-structure-based generation method

The ground-structure based layout optimization approach to finding an optimal strut and tie configuration for reinforcement design involves the following steps: in the first step, an array of bar elements that can take (concrete) compression, or (steel) tension, forces is assembled, interconnecting a grid of nodes (Fig. 2a). This layout of bars acts as potential strut and tie elements in a 'ground-structure', which may either contain all possible connections between nodes, or start with less dense (adjacent) connectivity and later proceed to increase connectivity via a 'member adding' process [51]. Boundary conditions and external loading are then applied at the relevant nodes for the structural problem. The bar members may be arranged in a way that allows for openings in the structural domain. Fig. 2a shows a low-density network of nodes and bar elements for illustrative purposes, but in practice significantly more nodes and bars would normally be used, providing a finer discretization of the structural domain.

Once the ground-structure has been constructed, a linear optimization problem is formulated to determine the minimum volume, fully

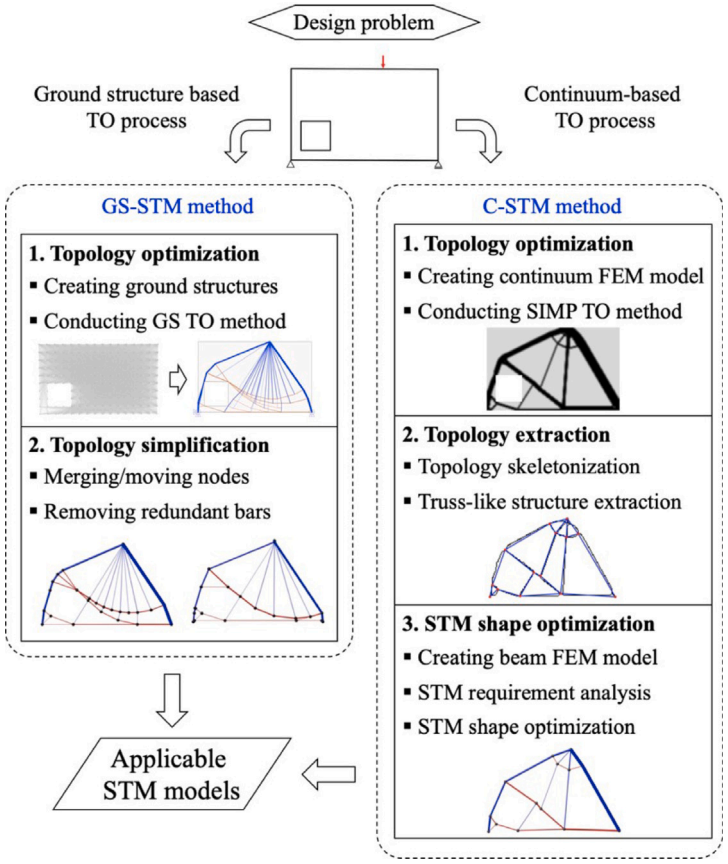

Fig. 1. ST model generation process of the GS-STM and C-STM methods.

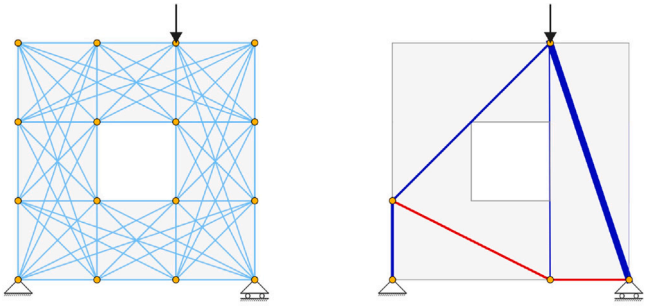

(a) A ground-structure (b) Resulting optimal structure

Fig. 2. The ground-structure truss layout optimization process, used to identify an optimal strut and tie configuration: (a) a ground-structure of (light blue) potential strut and tie bars, connecting (orange) nodes, subject to a downwards point load on the top and pin-roller supports at the base; (b) the resulting optimal configuration of (blue) concrete struts and (red) steel tie elements. (For interpretation of the references to colour in this figure legend, the reader is referred to the web version of this article.)

stressed, internal strut and tie arrangement that is in equilibrium with the externally applied loads for the given support conditions. This ground-structure layout optimization method was originally developed to identify optimal (minimum volume) truss structures [17,51–54]. Formally, for a problem involving a ground-structure comprising of n nodes and m potential members, the associated underlying linear optimization ('linear programming', LP) problem that involves finding the minimum volume strut-tie structure can be written as follows:

$$\min_{\mathbf{a},\mathbf{q}} V = \mathbf{l}^{\mathrm{T}}\mathbf{a}, \tag{1a}$$

$$\text{s.t.} \quad \mathbf{B}\mathbf{q} = \mathbf{f}, \tag{1b}$$

$$-\sigma_{\mathrm{c}}\mathbf{a} \le \mathbf{q} \le \sigma_{\mathrm{t}}\mathbf{a}, \tag{1c}$$

$$\mathbf{a} \ge \mathbf{0}, \tag{1d}$$

where V is the volume of the ST models; $\mathbf{l} = [l_1, l_2, \ldots, l_m]^{\mathrm{T}}$ is a vector of structure member lengths and $\mathbf{a} = [a_1, a_2, \ldots, a_m]^{\mathrm{T}}$ is a vector of member cross-sectional areas. Force equilibrium is imposed at nodes by Eq. (1b), where $\mathbf{B}$ is a $2n \times m$ matrix containing direction cosines, $\mathbf{q} = [q_1, q_2, \ldots, q_m]^{\mathrm{T}}$ is a vector of internal member forces, and $\mathbf{f} = [f_{1x}, f_{1y}, f_{2x}, f_{2y}, \ldots, f_{nx}, f_{ny}]^{\mathrm{T}}$ is a vector of externally applied loads. Yield constraints are enforced for each member by Eq. (1c), where σ_{t} and σ_{c} are limiting steel tensile and concrete compressive stresses respectively. Members are constrained to have zero or positive cross-section area in Eq. (1d). Since the objective function Eq. (1a) and all constraints are linear with respect to the optimization variables — member areas $\mathbf{a}$ and internal forces $\mathbf{q}$ — this is therefore an LP problem that can be solved efficiently using modern solvers, for problems involving millions of members, or more.

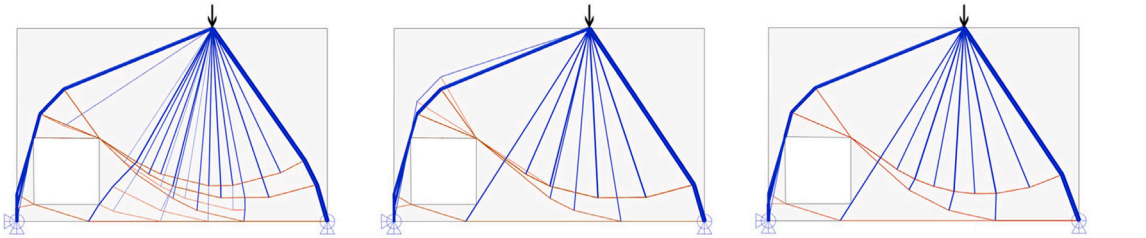

Fig. 3. The layout optimization method can include a joint cost and/or geometry optimization step, which can reduce the number of strut and tie elements, as well as reduce and move the nodes to produce a cleaner network of elements (after He and Gilbert [45]). Tensile and compressive forces are shown in red and blue respectively. (For interpretation of the references to colour in this figure legend, the reader is referred to the web version of this article.)

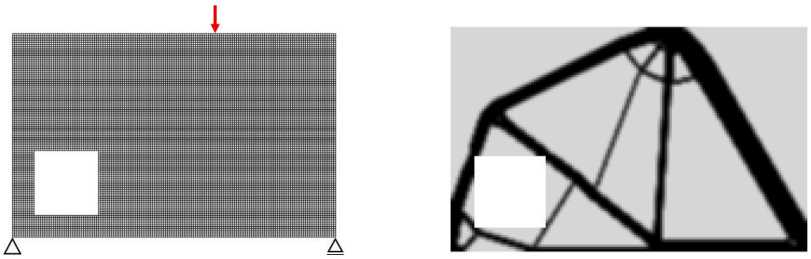

Fig. 4. Continuum-based topology optimization: (a) the continuum design domain (a plane FEM model) with loading and support conditions; (b) resulting optimized material distribution for subsequent STM model generation.

Once the internal forces are known from the optimization solution, they can be processed and plotted to determine the optimal strut and tie configuration, shown in Fig. 2(b). Members in the ground-structure that were not needed for the final solution are assigned zero areas and can be discarded. To avoid compressive struts or tensile reinforcement encroaching on the boundary perimeter, a concrete cover or inset can be applied to the structural domain before the analysis, such that the resulting struts and ties remain behind a given level of concrete cover.

To tidy up the strut and tie network, reduce member counts, and produce more buildable reinforcement designs, a joint cost may be added to remove overlapping members and reduce the complexity of the solution, and/or a geometry optimization post-process step can be used to merge and move nodes within the structural domain [45]. Fig. 3 demonstrates this, showing first the solution that results from the standard LP layout optimization step, then uses the joint cost method to remove overlapping members and penalize short elements, finally performing a geometry optimization step to move and merge nodes to reveal a clearer strut and tie system.

2.2. Continuum-based generation method

The STM model generation process for the continuum TO method (C-STM) consists of three main phases and is shown in Fig. 1. Unlike the GS-STM method, the topology optimization process is conducted using a continuum (plane or solid) finite element method (FEM) model, as shown in Fig. 4(a). The conventional density-based continuum TO procedure [55] is considered. In addition, SIMP material interpolation is adopted to determine the elemental Young's moduli as a function of the density design variables. The corresponding optimization problem is formulated as:

$$\min_{\boldsymbol{\rho}} c(\boldsymbol{\rho}) = \frac{1}{2}\mathbf{U}^{\mathrm{T}}\mathbf{K}\mathbf{U} = \frac{1}{2}\sum_{i=1}^{n} E_i(\rho_i)\mathbf{u}_i^{\mathrm{T}}\mathbf{k}_0\mathbf{u}_i, \tag{2a}$$

$$\text{s.t.} \sum_{i=1}^{n} \rho_i v_i \le V_0, \tag{2b}$$

$$\mathbf{K}\mathbf{U} = \mathbf{F}, \tag{2c}$$

$$0 \le \rho_i \le 1, i = 1, 2, \ldots, n, \tag{2d}$$

where $\mathbf{K}$ and $\mathbf{U}$ represent the global stiffness matrix and nodal displacement vector, respectively. They are assembled based on the elemental nodal displacement $\mathbf{u}_e$ and elemental stiffness matrix $\mathbf{k}_0$. The density ρ_i is associated with the i-th discretized finite element, while v_i and V_0 are the element volume and the maximal available volume of the optimized result. Also, $\mathbf{F}$ represents the applied nodal force. Using the SIMP method, the elemental Young's modulus $E_i(.)$ is calculated as:

$$E_i(\rho_i) = E_{\min} + \rho_i^p (E_{\max} - E_{\min}), \tag{3}$$

where, $E_{\max}$ is the Young's modulus of a solid element, $E_{\min}$ is a small value to prevent the global matrix $\mathbf{K}$ becoming singular, and p is a penalization factor ($p = 3$ in the current paper). Subsequently, the optimized material layouts are obtained by iteratively updating the densities using gradient-based optimization. The resulting optimized topology is shown in Fig. 4(b). For a detailed introduction of the classical TO method employing SIMP, readers are referred to the text by Bendsoe and Sigmund [55].

Since the optimized material distribution is represented via mesh densities, ST models, which are represented as discrete truss systems, cannot be obtained directly (as shown in the optimized material layout in Fig. 1). Here, in order to automatically generate discrete truss systems, the topology extraction method proposed in [43,44] is employed. In this systematic extraction procedure, the obtained material layout is simplified into an element skeleton via a thinning method. Complex topologies are transformed into relatively simple skeletons comprising far fewer pixels (or voxels in 3D cases), while the topological information remains unchanged. Based on the simplified skeleton, nodes and their connections can be effectively identified to represent truss-like systems.

The extracted truss-like structures are often statically and kinematically unstable truss structures. For the STM method, it is not necessary for the extracted structures to be stable trusses; however, the axial force equilibrium state is required to proceed with the STM design process. In order to obtain axial equilibrium forces, an STM shape optimization procedure [43,44] is conducted. The extracted truss-like structures are

analysed using beam finite element models. In this shape optimization process, the node positions of the extracted truss-like structures are taken as optimization variables. In addition, an index is formulated based on the ratio of member axial and shear forces F_{n} and F_{v}, as shown in Eq. (4):

$$\mathrm{STS} = \frac{1}{I}\sum_{i=1}^{I}\frac{F_{\mathrm{n}i}}{F_{\mathrm{n}i}+F_{\mathrm{v}i}} \tag{4}$$

where I indicates the total number of elements in the obtained truss-like structure. By constraining the STS index to a large value (STS $\geq$ 95%) in the shape optimization, the optimized structure approximates the axial force equilibrium state and can be used for subsequent STM analysis.

2.3. Key differences between STM generation methods

Although the two methods investigated herein can both generate suitable truss models for the STM method, key differences between them will now be briefly outlined. The C-TO approach, when employed for generating ST models, is based on the concept of compliance minimization (maximizing stiffness). In contrast, the GS-TO approach aims to minimize the volume of the structure while considering equilibrium equations and limiting stress constraints. This method relies on a plastic design formulation, ignoring the displacement field. Nonetheless, it can be shown that, under a single load case, the plastic design formulation involving volume minimization is equivalent to the minimum compliance design problem [56]. Additional key differences between the two methods are identified as follows:

(1) Design discretization. The GS-STM method starts from an initial truss ground-structure, typically containing a large number of truss bars. The C-STM method is based on a continuum finite element model, followed by shape optimization of a beam model. In terms of the optimization variables, practical cross-section sizes are adopted in the TO process when using the GS-STM method, whereas virtual material densities are obtained using the C-STM method. In addition, movement of joints in the truss models (truss-like structures in the case of C-STM and ground-structure members in the case of GS-STM) are also considered in the two methods. In the TO phase, the number of variables in the C-STM method is typically higher than in the GS-STM method, especially for 3D problems.

(2) Steps used to generate ST models. To obtain ST models applicable to the design of D-regions, both methods include procedures in addition to the TO process. In the case of the GS-STM method, the optimized result can contain a large number of members, with numerous members carrying small forces. These small cross-section members are generally insignificant when it comes to structural performance and inconvenient to construct in practice. To obtain more buildable designs, containing a smaller number of significant load carrying members, various simplification procedures can be adopted, such as utilizing joint costs and/or geometry optimization. Compared to the GS-STM method, the C-STM method involves two main steps to firstly transform the material densities into a truss-like system, which is subsequently transformed into an ST model where the axial forces are in static equilibrium.

(3) Computational cost. Considering practical application, the computational cost is also an important consideration when comparing the two methods. When using the GS-STM method ST models are generated from the optimized truss models. In contrast, the C-STM method involves the use of continuum finite element models in the TO process. The computational costs associated with the C-STM method can be relatively large, especially considering 3D cases where a large number of solid elements are typically involved. Although computing power is continuously increasing, it is still important to compare the computational costs of these two methods.

Table 1
Six aspects used to compare the two investigated STM generation methods.

Comparison aspect (goal)	Symbol
Strain energy of ST models (min)	s
Ultimate capacity (max)	p
Steel usage (min)	v
Material efficiency (max)	η
Computational cost (min)	t
Constructability (min)	c

3. Comparison procedures

To investigate the effectiveness of the two STM generation methods, a comparison procedure is proposed in this section. Differences between the methods affects both computational time and performance of the resulting STM designs. In order to provide a systematic comparison, six aspects are considered, as summarized in Table 1.

3.1. Evaluation aspects

- **Strain energy of ST models** s
  As external applied loads should if possible be transferred through a structure with the least forces and deformations, in [4,30] the strain energy associated with truss models was used as an ST model evaluation criterion. In the current study, the strain energy of the generated truss-like structures is therefore used as a comparison aspect for the two methods, as indicated in Eq. (5):

$$\begin{aligned} s &= 0.5\sum_{i=1}^{I}F_{\mathrm{n}i}U_{\mathrm{n}i} = 0.5\sum_{i=1}^{I}F_{\mathrm{n}i}l_{\mathrm{n}i}\epsilon_i \\ &= 0.5\sum_{i=1}^{I}F_{\mathrm{n}i}l_{\mathrm{n}i}\frac{F_{\mathrm{n}i}}{a_i E} = 0.5\sum_{i=1}^{I}F_{\mathrm{n}i}l_{\mathrm{n}i}\frac{f_{\mathrm{y}}}{E} \end{aligned} \tag{5}$$

  where f_{y} and E denote the material yield strength and Young's modulus of steel, respectively. Since the generated truss-like models are unstable truss structures, analysed using a beam FEM model, only the part based on the axial forces F_{n} and displacement U_{n} is considered when calculating the strain energy. The forces are calculated considering an applied load of 1 N. Also, l_i and ϵ_i denote the length and strain of the i-th member of the ST model. Finally, a_i is the cross-sectional area calculated from the internal force, with $a_i = F_{\mathrm{n}i}/f_{\mathrm{y}}$.
- **Performance of ST designs** p
  Evaluating the structural performance of the resulting ST designs provides a more direct way of comparing the efficacy of the two STM generation methods. Nonlinear features, such as concrete cracking and rebar fracturing, are not implemented in the two investigated STM generation methods, and these also do not provide a robust means of calculating load-carrying capacity [16]. In order to achieve this, a NLFEA evaluation procedure [43,44,50] is employed, with cracking and crushing of the concrete and yielding and fracturing of the steel both considered. By specifying the loading scheme and convergence criteria, a NLFEA is conducted and the simulation result allows determination of the load-carrying capacity and mode of failure. In a recent publication by [57] it is found that the ratio of experimentally found load resistance and the numerically simulated resistance, for the adopted finite element approach, has a mean of 1.075 and a coefficient of variation of 0.118. This means that the results of the finite element analyses are on the conservative side and that the accuracy of finite element results is sufficient to use them as a reference for the strut and tie model results. The performance of the two investigated methods can then be systematically compared. For this aspect, the ultimate capacity p (peak load point) is considered as an index, which should be larger than the design load p_0.

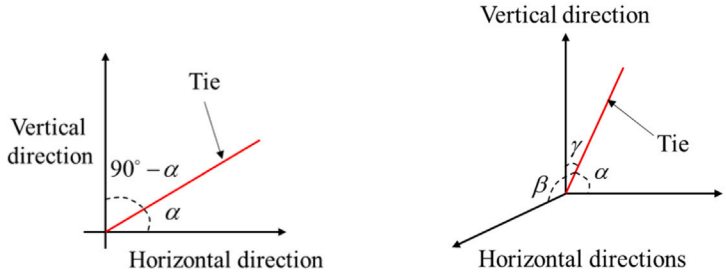

(a) 2D case (b) 3D case

Fig. 5. Angles used in the calculation of tie inclination angle θ.

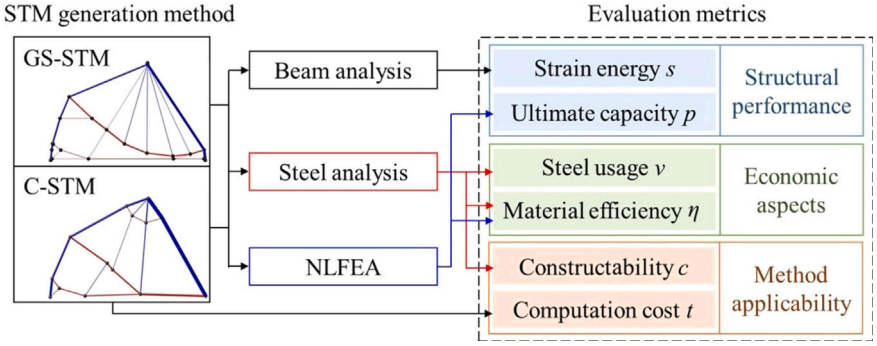

Fig. 6. Comparison procedure for the generated ST models, involving six metrics.

- **Steel usage** v
  In addition to structural performance, material usage is also an important aspect when considering the STM designs. Commonly, concrete is used to fill the whole design domain and thus there is effectively no difference between the two investigated methods with respect to concrete usage. In the current study, the steel usage of the resulting STM designs is therefore considered as a comparator. The steel usage is calculated from Eq. (6), where only tensile members are considered.

$$v = \sum_{i=1}^{I} a_i l_i \tag{6}$$

- **Material efficiency** η
  To provide a further indicator of material efficiency of the generated STM designs, a dimensionless ratio η [43] is defined. In the current work, the η ratio is used to indicate the degree of utilization of the steel material, as shown in Eq. (7):

$$\eta = \frac{p}{p_0} \Big/ \frac{v}{v_0} \tag{7}$$

  where p_0 indicates the prescribed design load and v_0 is the steel volume based on a specific reinforcement ratio. Considering the steel usage in common reinforced concrete structures, a reinforcement ratio of 1% is applied in the current paper. A larger material efficiency ratio indicates that a more efficient STM design has been obtained.
- **Computational cost** t
  Considering practical application of the two investigated methods, the computational cost is also an important aspect. Here, the total computational time t of the given investigated method is considered. For both methods time is expended in the topology optimization phase (t_{TO}) and in extra post-processing steps (t_{e}). The total computation time includes both these, i.e., $t = t_{\mathrm{TO}} + t_{\mathrm{e}}$.
- **Constructability** c
  For the generated ST models, detailing steps are always needed to transform the design into practically constructable structures. The generated ST model involves ties with different lengths and cross-sections. In addition, the obtained ties are usually placed in inclined orientations. Commonly, rebars are designed using a sectional analysis, with rebars then placed in a vertical–horizontal manner. The varying ties and inclined placements lead to difficulties fixing the steel in practice. In the current paper, two main aspects are considered to evaluate the constructability of STM designs, including rebar angle and steel cross-section uniformity; also, rebars of similar length and section size are desired.
  Considering these aspects, a constructability index c is defined to quantitatively compare the investigated methods, as shown in Eq. (8):

$$c(\theta) = \sum_{i}^{I} (\tan(\theta_i) + 0.01) \frac{l_i}{l_k} \frac{\min(|a_i - a_j^{\mathrm{set}}|)}{a_{\max} - a_{\min}} \quad (j = 1, \ldots, J) \tag{8}$$

  where the index c is defined based on the variation of the cross sections of the ties and their positions and lengths. In this equation, θ indicates the position angle (angle to the horizontal and vertical directions), as defined in Eq. (9):

$$\theta = \begin{cases} \min(\alpha, 90 - \alpha) & \text{(2D case)} \\ \min(\alpha, 180 - \alpha, \beta, 180 - \beta, \gamma, 180 - \gamma) & \text{(3D case)} \end{cases} \tag{9}$$

  where angles α, β and γ are indicated in Fig. 5. Also, l_k is the representative length of the design problem, which is calculated as $l_k = \sqrt[2]{a_s}$ (or $\sqrt[3]{V_s}$ for 3D cases); a_i and l_i indicate the size and length of ith tie member; $a_{\max}$ and $a_{\min}$ are the maximum and minimum sizes of the obtained ties. In addition, a cross-section set a^{set} is prescribed to represent the desired clustering of rebar sizes. In the current paper, the cross section set a^{set} consists of J parts (where $J = 5$ in the current paper), in the range between $a_{\min}$ and $a_{\max}$.

3.2. Evaluation procedure

The metrics proposed in the previous section are used to form the basis of the evaluation procedure shown diagrammatically in Fig. 6,

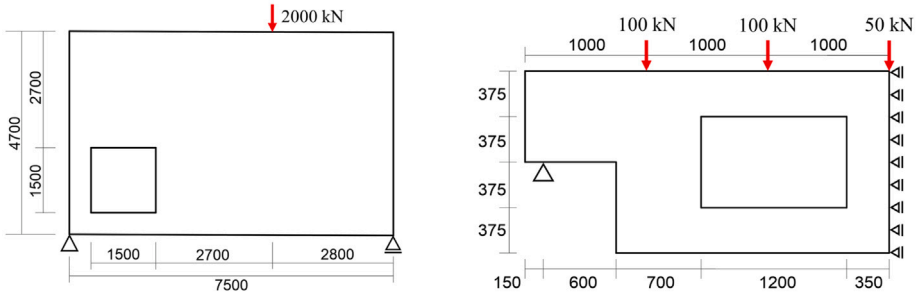

(a) Deep beam with an opening (b) Dapped-end voided beam

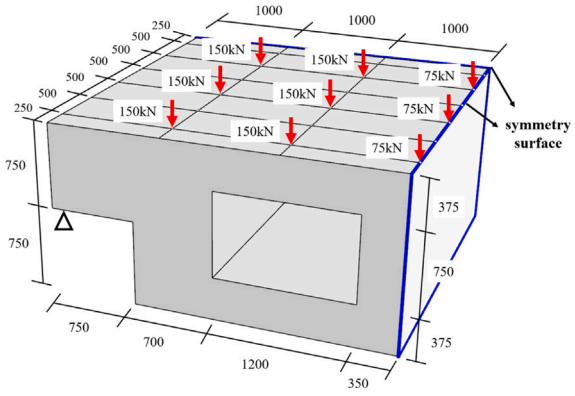

(c) 3D dapped-end voided slab

Fig. 7. Three typical D-regions to compare the performance of the GS-STM and C-STM methods. The corresponding design loads for the investigated cases are also indicated.

facilitating objective comparison of the two STM model generation methods. Using the generated ST models, beam analysis and NLFEA models are created and run to establish structural performance indicators s and p. Next, economic aspects, based on steel usage v and material efficiency η, are considered. Finally, the applicability of the two methods is evaluated, considering constructability c and computation cost t.

4. Case studies of three typical D-regions

Three typical reinforced concrete design problems incorporating D-regions are now investigated, including two 2D cases and a 3D case. Basic details of these cases are introduced below. Firstly, the two methods are used to generate ST models for a deep beam with an opening. Deep beams are typical structural components that are used to support heavy loads, often over long spans. The load transfer mechanism of this structural type is relatively complex, and becomes even more complex when there is an opening. Next, a dapped-end voided beam case, often used in the construction of bridges, is investigated. Finally, a voided slab case in a 3D configuration is investigated to further compare the applicability and performance of the two methods. The geometries of these investigated cases are shown in Fig. 7. For both investigated methods, the STM generation process starts with a TO process; thus, the design discretizations (ground-structures and continuum meshes) employed are shown in Fig. 8. Further details of the generated STM models and the results obtained are presented in the following sections.

4.1. Deep beam with opening

In this section, the two investigated methods are used to generate ST models for the deep beam problem shown in Fig. 7(a), which indicates the geometry, loading and boundary conditions. Note that the discontinuity introduced by including an opening in the deep beam can be expected to lead to a relatively complex load transfer mechanism.

Firstly, for the GS-STM method, an initial ground-structure that included the opening was generated for use in the optimization process, as shown in Fig. 8(a). Nodal spacings of between 150 mm and 300 mm were used in the optimization runs, though for sake of clarity a spacing of 400 mm is shown in Fig. 8(a). Material stress limits of 40 MPa for the concrete and 500 MPa for the reinforcing steel were assumed. Simply supported boundary conditions were applied as indicated, with a point load applied at the top face. Concrete cover of 70 mm was assumed around the edges of the domain, to ensure the tie forces were carried well inside the structure, and also for practical reasons. For a given nodal spacing the joint cost was varied to give solutions with different numbers of tensile members, ranging from 5 to 59. A typical example of one of the optimized layouts obtained is shown in Fig. 9. All solutions were post-processed with up to 10 geometry optimization iterations. Since the problem involves truss elements from the outset, the solution obtained could be directly used to form a suitable ST model.

Next, the C-STM method was used for STM generation. In this case, a continuum FEM with a mesh size of 50 mm was created for the deep beam, as shown in Fig. 8(b). The classical SIMP TO method [55] was used to obtain a solution, with the filter radius and volume fraction set to 2×50 mm and 25% respectively. The optimized material distribution is shown in Fig. 10(a) and the corresponding principal stress contour is shown in Fig. 10(b). Following topology extraction and subsequent shape optimization, a C-STM can be generated, as shown in Fig. 11.

Based on the two obtained ST models, the required rebar cross sections can be determined and the performance of the resulting ST designs can be simulated via NLFEA. In the interests of brevity, for all NLFEA simulation settings and employed solution strategies, readers are referred to previous papers by Xia et al. [43,44,50]. The load–displacement curves of the two designs are shown in Fig. 12, where the displacement is measured at the loading point. The two STM designs both result in safe designs, with the computed ultimate load capacities being larger than the specified design load. Based on the

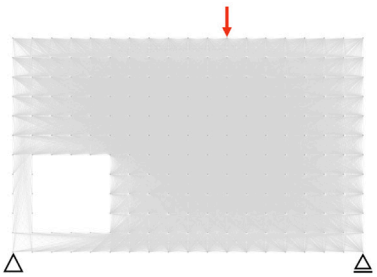

(a) Deep beam with an opening (GS method, 53000 truss elements) shown for a nodal spacing of 400 mm

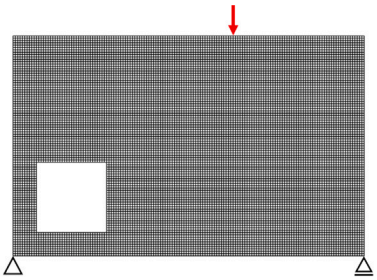

(b) Deep beam with an opening (C-STM method, 13200 continuum mesh elements)

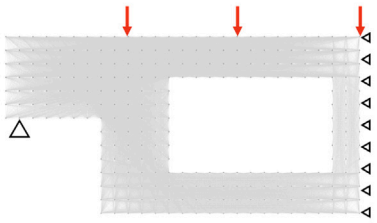

(c) Dapped-end voided beam (GS-STM method, 143000 truss elements)

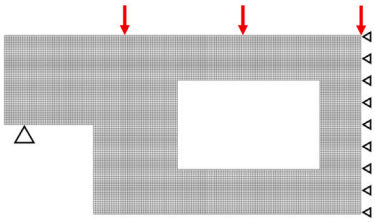

(d) Dapped-end voided beam (C-STM method, 13500 continuum mesh elements)

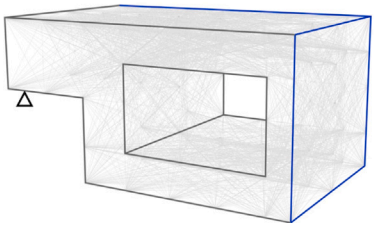

(e) 3D dapped-end voided slab (GS-STM method, 10000 truss elements)

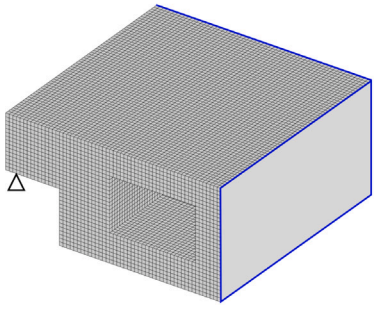

(f) 3D dapped-end voided slab (C-STM method, 72900 continuum mesh elements)

Fig. 8. Domain discretizations employed for the three investigated cases.

simulation results, concrete cracks occur at the opening corner and then progressively propagate; a portion of reinforcement then starts to yield. The concrete cracking and rebar yielding lead to stress redistribution, with more parts of the structure then activated. At the final loading stage, large rebar strains are observed and the structure fails due to steel fracturing. Crack patterns at the ultimate loading point for the two designs are shown in Fig. 13; these indicate that the two designs lead to similar crack distributions. In both cases a main diagonal crack propagates from the upper right corner of the opening to the loading plate.

Results from the evaluation process for the two designs are summarized in Table 2. The generated ST models require similar quantities of steel, and have similar ultimate load-carrying capacities (though the capacity of the GS-STM design is 6.1% higher than that of the C-STM design). The material efficiencies are also similar, though a slightly higher efficiency is achieved by the C-STM design (considering both load-carrying capacity and steel usage). Considering constructability, the number of tensile members in the GS-STM and C-STM designs is 9 and 11, respectively, leading to similar constructability indices for the two designs. The main difference lies in computational cost, which was significantly lower in the case of the GS-STM design.

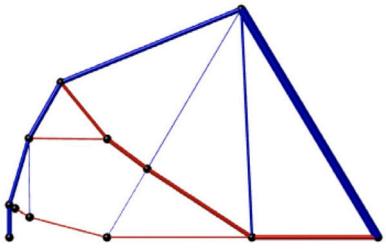

Fig. 9. Deep beam with opening: one of the optimized layouts based on the GS TO method. Red and blue lines indicate tensile and compressive members. Line thickness indicates the relative magnitude of the member forces. (For interpretation of the references to colour in this figure legend, the reader is referred to the web version of this article.)

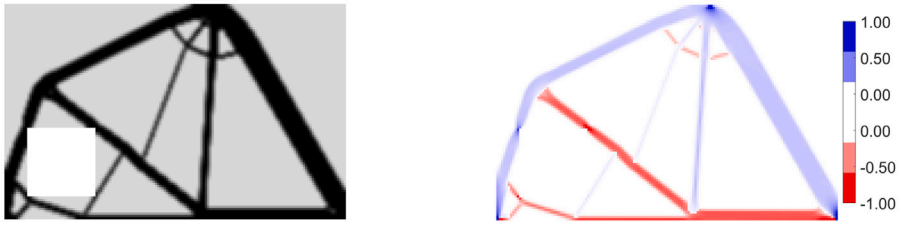

(a) Topology optimization result (b) Resulting principal stress contour

Fig. 10. Deep beam with opening: continuum-based topology optimization result. Red and blue elements indicate tensile and compressive regions, respectively. Colour intensity indicates the normalized principal stress magnitude. (For interpretation of the references to colour in this figure legend, the reader is referred to the web version of this article.)

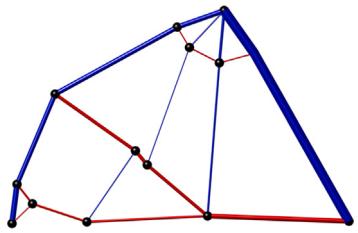

Fig. 11. Deep beam with opening: generated C-STM. Red and blue lines indicate struts and ties, respectively. Line thickness is proportional to the magnitude of the axial forces. (For interpretation of the references to colour in this figure legend, the reader is referred to the web version of this article.)

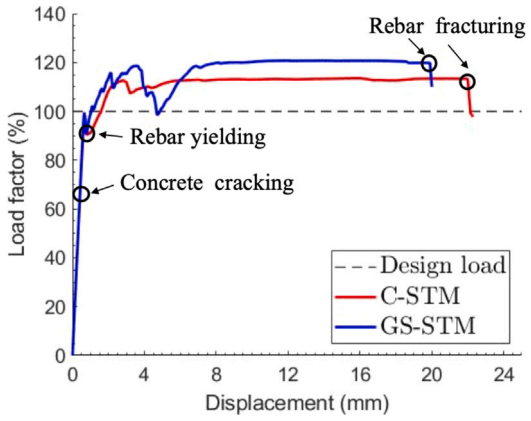

Fig. 12. Deep beam with opening: load–displacement curves for the two STM designs.

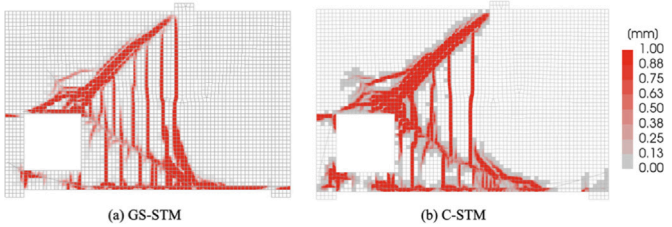

Fig. 13. Deep beam with opening: simulated crack patterns for the two designs at the ultimate load point. A large crack is observed to propagate from the corner of the opening to the loading plate, with cracks also distributed along the length of the lower rebar.

4.2. Dapped-end voided beam

In this section, the two investigated STM generation methods are applied to the dapped-end voided beam shown in Fig. 7(b), which indicates the geometry, loading and boundary conditions. As with the deep beam case considered previously, an initial ground-structure was generated for the GS-STM method, as shown in Fig. 8(c), in this case showing a nodal spacing of 110 mm. A ground structure was generated that incorporated the opening, with a cover offset defined around the internal opening and outer perimeters. A single horizontal roller support was placed at the left hand corner, with vertical roller supports placed along the right side of the design domain to represent a line of symmetry; also three point loads were applied to the top face as indicated in Fig. 8(c). The same concrete and steel material properties as used for the previous deep beam example were used. In the optimization a uniform nodal spacing of 70 mm was employed, with the joint cost varied to give solutions containing between 8 and 37 tensile members. Geometry optimization was again used for a maximum of 10 iterations. A sample optimized result is shown in Fig. 14.

Table 2
Deep beam with opening: evaluation results for the two designs.

Index	GS-STM	C-STM
Strain energy s (N mm)	16.9	20.5
Ultimate capacity p/p_0	1.21	1.14
Steel usage v (10^6 mm^3)	10.9	10.1
Material efficiency η	18.30	18.63
Computational cost t (s)	0.8	51
Constructability c	0.060	0.069

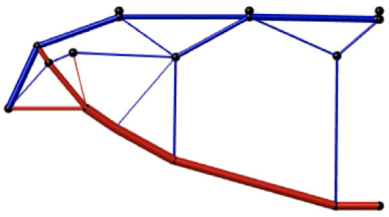

Fig. 14. Dapped-end voided beam: optimized layout based on GS-TO method. Red and blue lines indicate the tensile and compressive members. Line thickness is proportional to the magnitude of the axial forces. (For interpretation of the references to colour in this figure legend, the reader is referred to the web version of this article.)

Next, the C-STM generation method was applied, using the FEM model shown in Fig. 8(d). In this case, a finite element mesh size of 15 mm was used, and, for the TO process, a filter radius of 2×15 mm and volume fraction of 25% were used. The optimized material distribution is shown in Fig. 15(a) and the corresponding principal stress contour is shown in Fig. 15(b). The C-STM shown in Fig. 16 was generated by conducting topology extraction and shape optimization.

Again, analysis models were then created based on the two designs generated. The load–displacement curves obtained from the NLFEA simulations are shown in Fig. 17, where the displacement is measured at the location of the point load located on the line of symmetry. The ultimate load capacity (p/p_0) of the two designs was found to be 1.15 (GS-STM) and 1.12 (C-STM), indicating that both designs are safe. In addition, a plastic response can be observed for both designs, with a clear loading plateau evident in the load–displacement curves. Based on

(a) Topology optimization result (b) Resulting principal stress contour

Fig. 15. Dapped-end voided beam: continuum-based topology optimization result. Red and blue elements indicate tensile and compressive regions, respectively. Colour intensity indicates the normalized principal stress magnitude. (For interpretation of the references to colour in this figure legend, the reader is referred to the web version of this article.)

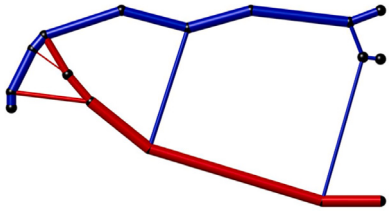

Fig. 16. Dapped-end voided beam: generated C-STM. Red and blue lines indicate struts and ties, respectively. Line thickness is proportional to the magnitude of the axial forces. (For interpretation of the references to colour in this figure legend, the reader is referred to the web version of this article.)

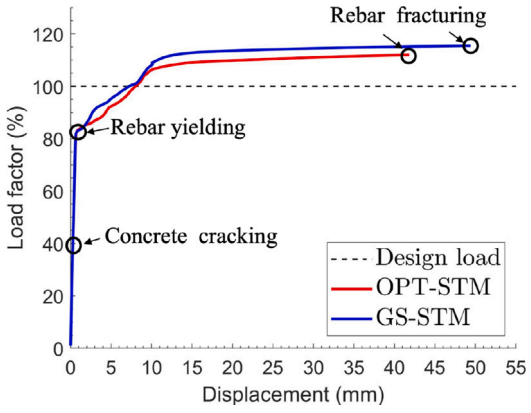

Fig. 17. Dapped-end voided beam: load–displacement curves for the two STM designs.

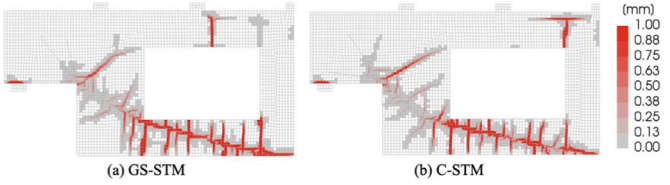

Fig. 18. Dapped-end voided beam: simulated crack patterns for the two designs at the ultimate load point, each showing similar crack distributions. Cracks are spread along the length of the main tensile reinforcement element located towards the bottom of the beam.

the simulation results, the beam is initially very stiff under loading. As the steel bars yield, cracks in the concrete appear perpendicular to the directions of the rebars. During the final loading phase, similar to the previous case, the structure failed due to steel fracture. Simulated crack patterns at the ultimate loading point are shown in Fig. 18, indicating that the two designs lead to similar crack distributions.

Table 3
Dapped-end voided beam: evaluation results for the two designs.

Index	GS-STM	C-STM
Strain energy s (N m)	38.60	37.99
Ultimate capacity p/p_0	1.15	1.12
Steel usage v (10^6 mm^3)	1.51	1.58
Material efficiency η	11.55	10.80
Computational cost t (s)	13	181
Constructability c	0.039	0.031

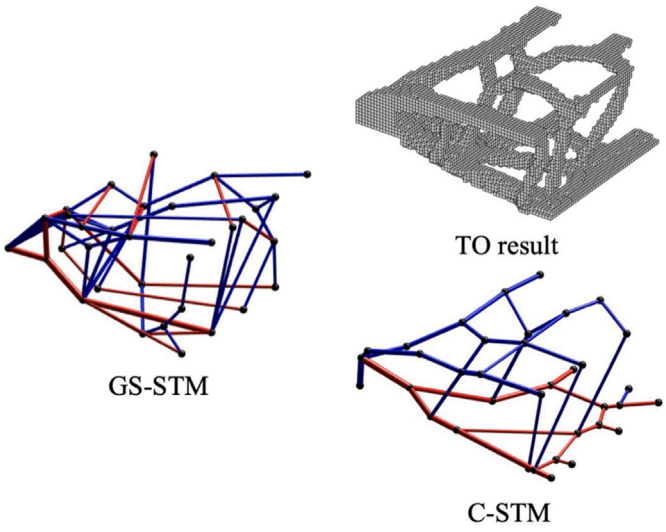

Fig. 19. 3D dapped-end voided slab: obtained ST models based on the GS-STM and C-STM methods.

Results from the evaluation process for the two designs are summarized in Table 3. In addition to having a slightly higher load capacity, the steel usage of the GS-STM design is 4.4% lower than the C-STM design; thus a higher material efficiency factor is also obtained via the GS-STM method. Similar strain energies are obtained when using the GS-STM and C-STM methods. Compared to the GS-STM design, the C-STM design has fewer ties and hence a slightly lower constructability factor. Again the GS-STM design required significantly less computational time to generate.

4.3. 3D dapped-end voided slab

The two investigated STM methods are now applied to the design of the 3D dapped-end voided slab shown in Fig. 7(c). Compared to the dapped-end voided beam considered in the previous section, the geometry of the 3D case is generated by extruding the 2D voided beam in an out-of-plane direction. However, in this case, a roller support is present at the bottom left corner, with planar roller supports at planes

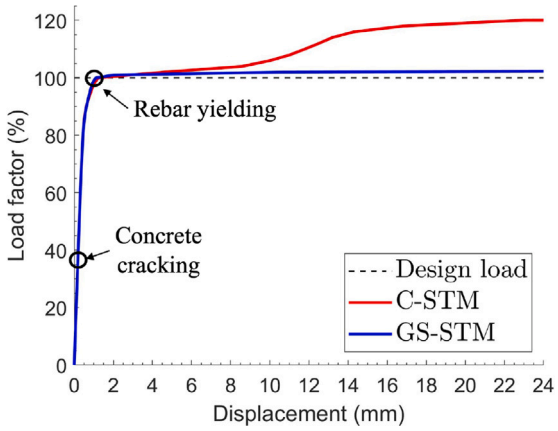

Fig. 20. 3D dapped-end voided slab: load–displacement curves for the two ST designs.

Table 4
3D dapped-end voided slab: evaluation results for the two designs.

Index	GS-STM	C-STM
Strain energy s (N m)	202.3	194.6
Peak capacity p/p_0	1.03	1.22
Steel usage v (10^6 mm^3)	11.7	11.1
Material efficiency η	8.05	9.99
Computational cost t (s)	16	1040
Constructability c	0.398	0.167

of symmetry as indicated in the figure. As also indicated, the slab is subject to distributed loading on the top surface, discretized via nine concentrated loads in the STM analysis. The models developed for the GS-STM and C-STM generation methods are shown in Fig. 8.

For the GS TO process a ground-structure was constructed within the volumetric domain using a nodal grid spacing of between 150 mm and 300 mm; grids finer than this were found to lead to overly complex force systems. As with previous examples, a joint cost was used in the ground structure layout optimization step, prior to a geometry optimization step (up to 5 geometry optimization iterations were used in this case). This produced solutions containing between 12 and 43 tensile members; different model configurations are discussed further in Section 5. For the C-STM TO process a filter radius of 3×50 mm was used together with a volume fraction of 15% when seeking an optimized structure. The C-STM TO result and resulting STM model are shown in Fig. 19, alongside the generated GS-STM model.

Once again NLFEA was conducted to evaluate the performance of the two STM designs, with the resulting load–displacement curves shown in Fig. 20; crack patterns at the ultimate load point are shown in Fig. 21. It is found that the two designs fail due to fracturing of the steel at the peak load. In this case the load capacity of the C-STM design is observed to increase at large deformations.

Evaluation results for the two designs are summarized in Table 4. It is again evident that the two designs are both safe, with the ultimate capacity being larger than the design load. In the case of this example the C-STM design provides a higher ultimate load capacity ($p/p_0 = 1.22$ compared with $p/p_0 = 1.03$). Compared to the C-STM design, the strain energy and steel usage associated with the GS-STM design are slightly higher, and the material efficiency ratio lower. In addition, a higher constructability index is observed for the GS-STM design. However, a relatively large computation cost is observed for the C-STM method, with the 3D topology optimization process consuming a high proportion of the overall computational time.

5. Influence of input parameters on STM performance

Adjustment of the input parameters used in the two ST generation methods is likely to produce STMs with differing member layouts,

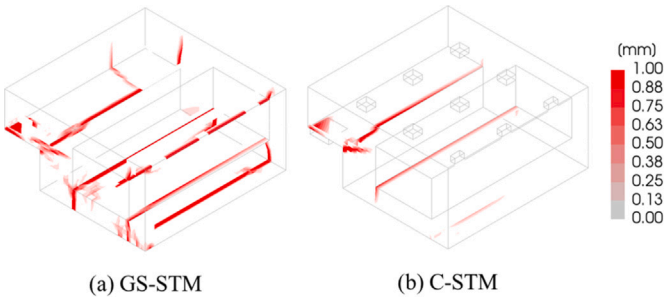

Fig. 21. 3D dapped-end voided slab: simulated crack patterns of the two designs at the ultimate load point. Large cracks distributed over the span are observed for both designs.

which in turn are likely to have differing performance characteristics. The influence of differing rebar locations on the performance of STM designs was investigated in [16]; here the influence of the input parameters on the STM designs will be considered. However, the abrupt changes in structural response observed in [16] were not observed here, suggesting a level of robustness in the optimal ST configurations obtained.

Considering the GS-STM generation method, changing the number of nodal divisions and the joint cost parameter can be used to generate ST models containing different numbers of members. Considering the C-STM generation method, the generated ST models are affected by parameters in the TO and truss extraction process. The influence of method parameters on C-STMs was discussed in [43]. The adopted volume fraction and the filter radius affect the obtained optimized material distributions in the TO process, and the merging length of short members affects the extracted truss-like models. Specifically, by using a relatively large filter radius and merging length, and small volume fraction, ST models containing fewer members can be obtained.

In this study, the previously investigated deep beam with opening case is initially considered (see Section 4.1). Firstly, C-STMs generated using different settings are shown in Fig. 22. It is found that varying the volume fraction and filter radius leads to between 8 and 14 ties being present in the generated C-STMs, though it is evident that the overall distribution of ties remains broadly similar in all cases. Using the GS-based generation method it is possible to vary the number of ties more freely, as shown in Fig. 23, where the GS-STM models contain between 6 and 59 ties, controlled by varying the joint cost j and nodal division spacing d. However, once again the overall distribution of ties remains broadly similar in all cases.

The proposed evaluation process has been conducted for all STM designs obtained using the two generation methods; see Table 5. Again, all designs based on the presented ST model configurations are safe, with the ultimate capacity being larger than the design load and failure due to rupturing of the steel. Considering averaged values, a slightly higher mean load capacity p/p_0 is observed for the GS-STM designs compared to the C-STM designs. In addition, a slightly lower volume of steel v is required when using the GS-STM method. Furthermore, the mean strain energy s is lower for the GS-STM designs, and a higher material efficiency ratio η is also observed. In terms of applicability, smaller constructability indices c are obtained in the case of the C-STM designs, though the associated computation times t are higher.

Next, max–min normalization results are plotted in Fig. 24, with the evaluated metrics from Table 1 plotted based on the number of tensile members (ties). The strain energies of the generated STM models decrease with increasing numbers of tensile members, and stiffer results can be obtained with more refined STM models. In addition, lower strain energies are observed when the GS-STM generation method is used. The ultimate load capacity p and material efficiency η also improve when more refined STM models are used, while the steel usage v reduces. This is because increasing the number of ties results

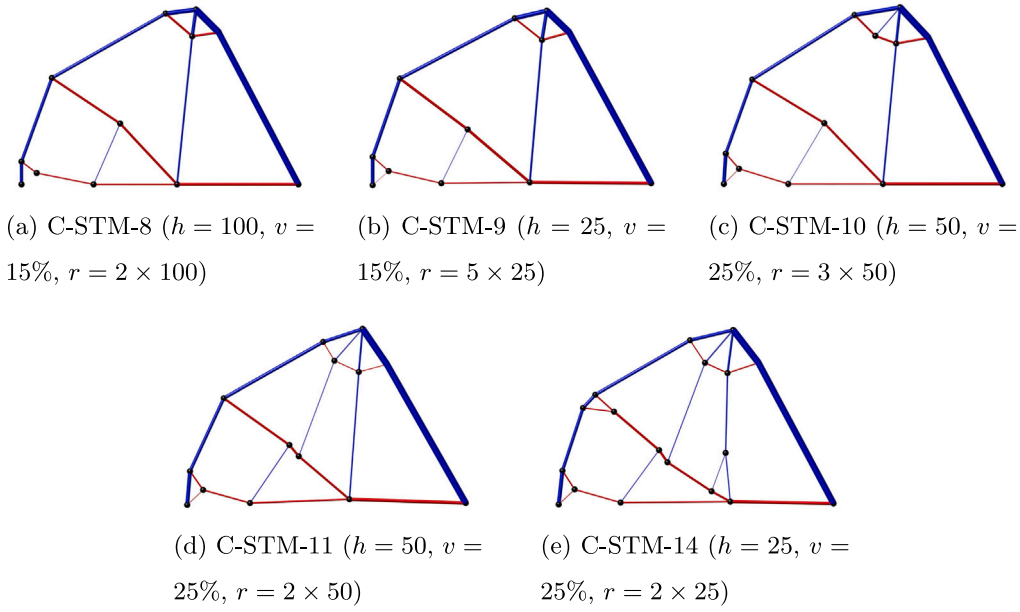

(a) C-STM-8 ($h = 100$, $v = 15\%$, $r = 2 \times 100$)

(b) C-STM-9 ($h = 25$, $v = 15\%$, $r = 5 \times 25$)

(c) C-STM-10 ($h = 50$, $v = 25\%$, $r = 3 \times 50$)

(d) C-STM-11 ($h = 50$, $v = 25\%$, $r = 2 \times 50$)

(e) C-STM-14 ($h = 25$, $v = 25\%$, $r = 2 \times 25$)

Fig. 22. Deep beam with opening: generated C-STMs with different number of members. The adopted parameters (mesh size, volume fraction and filter radius) in the C-STM method are indicated as h (mm), v and r (mm), respectively.

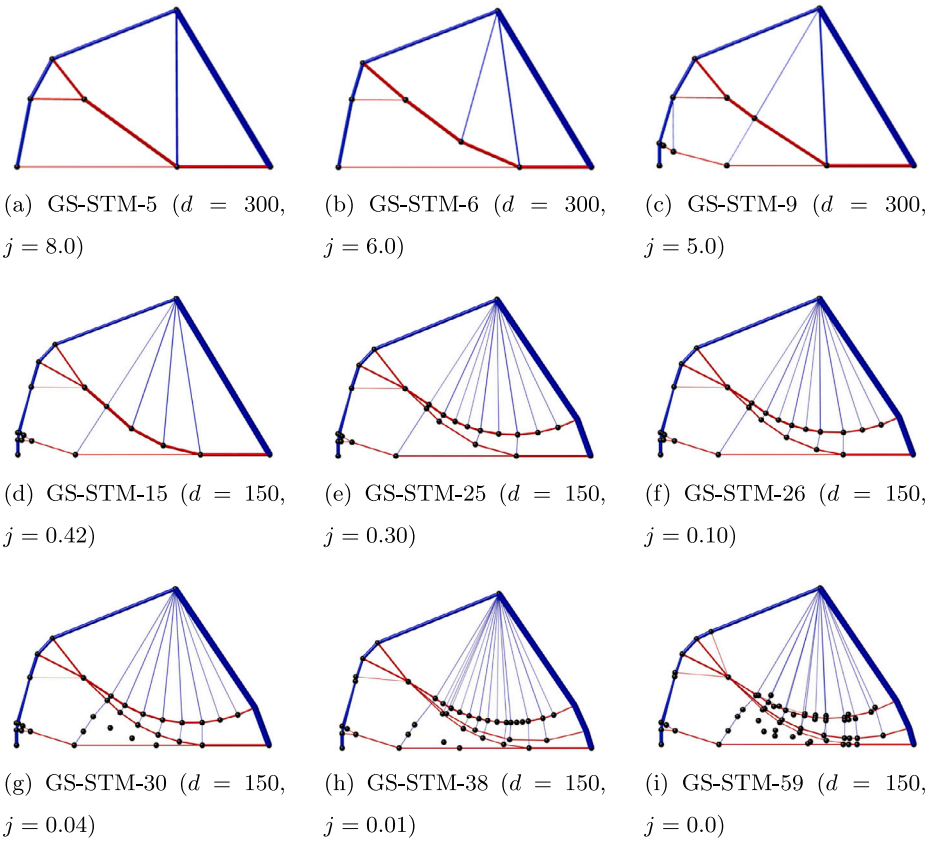

(a) GS-STM-5 ($d = 300$, $j = 8.0$)

(b) GS-STM-6 ($d = 300$, $j = 6.0$)

(c) GS-STM-9 ($d = 300$, $j = 5.0$)

(d) GS-STM-15 ($d = 150$, $j = 0.42$)

(e) GS-STM-25 ($d = 150$, $j = 0.30$)

(f) GS-STM-26 ($d = 150$, $j = 0.10$)

(g) GS-STM-30 ($d = 150$, $j = 0.04$)

(h) GS-STM-38 ($d = 150$, $j = 0.01$)

(i) GS-STM-59 ($d = 150$, $j = 0.0$)

Fig. 23. Deep beam with opening: generated GS-STMs with different number of members, by changing joint cost value j and the nodal spacing d. Lines with very small cross sections are not displayed.

in greater steel coverage, enhancing the ability of the structure to effectively prevent the initiation of tensile cracks. Considering practical aspects, the constructability index increases as the numbers of tensile members increase, with the computational cost remaining relatively low in the case of the GS-STM method. Conversely, significant variations in computational time are observed when the C-STM method is used, something that could possibly be addressed by using different termination criteria.

Next the 3D dapped-end voided slab case is investigated (see Section 4.3), varying the inputs in the same way as with the previous example. Thus, for this example the TO method inputs were varied to obtain STM models with between 15 and 20 tensile members, while the

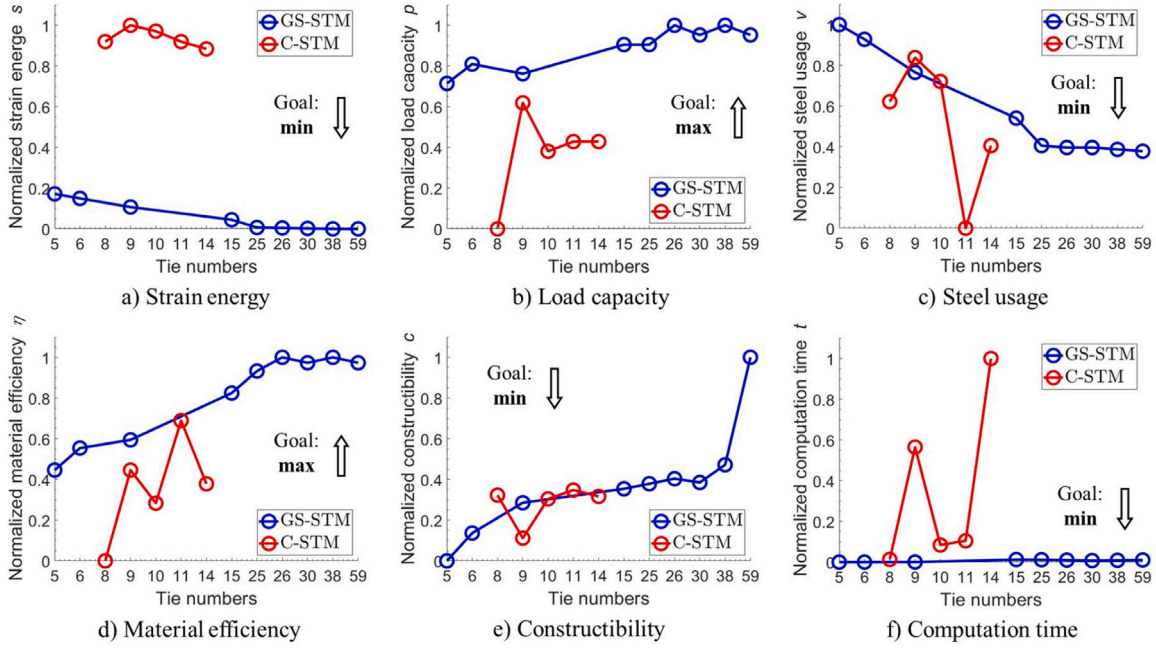

Fig. 24. Deep beam with opening: max–min normalization of evaluation results for STMs with differing numbers of ties. The arrows in the subfigures indicate the goal of the corresponding metrics.

Table 5
Deep beam with opening: evaluation results for STMs with different members of ties.

Method	Ties	s	p/p_0	v	η	c	t
GS-STM	5	17.19	1.20	11.17	17.75	0.014	0.66
	6	17.09	1.22	11.09	18.15	0.036	0.70
	9	16.90	1.21	10.91	18.30	0.060	0.86
	15	16.62	1.24	10.66	19.16	0.071	6.7
	25	16.45	1.24	10.51	19.54	0.075	6.3
	26	16.44	1.26	10.50	19.82	0.079	5.4
	30	16.43	1.25	10.50	19.72	0.076	4.3
	38	16.42	1.26	10.49	19.81	0.090	4.9
	59	16.42	1.25	10.48	19.71	0.175	5.7
mean	–	16.66	1.24	10.70	19.11	0.075	3.95
std dev.	–	0.30	0.021	0.26	0.77	0.042	2.50
C-STM	8	20.54	1.05	10.75	16.11	0.066	7
	9	20.90	1.18	10.99	17.73	0.032	272
	10	20.77	1.13	10.86	17.17	0.063	41
	11	20.54	1.14	10.06	18.63	0.070	51
	14	20.38	1.14	10.51	17.96	0.065	481
mean	–	20.63	1.13	10.63	17.52	0.059	170
std dev.	–	0.19	0.043	0.33	0.85	0.014	181

GS method inputs were varied to obtain STM models with between 12 and 43 tensile members, as shown in Fig. 25 and Fig. 26, respectively.

Evaluation results for the generated STMs are summarized in Table 6. Again, safe STM designs are obtained, with the predicted ultimate load capacities being larger than the prescribed design load. In this case, the average strain energy of the GS-STM designs is smaller than that of the C-STM designs. However, a slightly larger average ultimate load capacity is obtained for the C-STM designs (1.18) compared to the GS-STM designs (1.13), amounting to a difference of approx. 4.4%. However, the steel consumed by the C-STM designs is 4.5% larger than that consumed by the GS-STM designs, such that the averaged material efficiency ratios are similar. Compared to C-STM designs (where $c = 0.148$), larger constructability indices are obtained for the GS-STM designs ($c = 0.518$); however, the computation time required when using the C-STM method is much higher due to the computationally intensive nature of the 3D topology optimization process.

Table 6
3D dapped-end voided slab: evaluation results for STMs with differing numbers of ties.

Method	Ties	s	p/p_0	v	η	c	t
GS-STM	12	218.91	1.09	12.9	7.70	0.434	1.08
	19	202.27	1.03	11.7	8.05	0.398	1.07
	21	202.15	1.04	11.7	8.10	0.405	1.05
	23	210.99	1.20	12.2	8.95	0.665	9.85
	26	193.10	1.20	11.0	9.96	0.593	9.92
	30	188.19	1.16	10.8	9.78	0.525	9.97
	35	188.16	1.14	10.8	9.64	0.648	10.0
	39	186.74	1.14	10.6	9.79	0.542	9.84
	43	186.12	1.14	10.5	9.91	0.450	10.1
mean	–	197.40	1.13	11.35	9.10	0.518	6.98
std	–	11.17	0.058	0.77	0.86	0.096	4.44
C-STM	15	219.88	1.20	12.6	8.66	0.135	1055
	17	203.97	1.14	11.7	8.89	0.083	1063
	18	198.82	1.04	11.4	8.34	0.170	1069
	19a	194.60	1.22	11.1	9.99	0.167	1040
	19b	210.61	1.30	12.1	9.81	0.120	1045
	20	214.82	1.16	12.3	8.59	0.216	1075
mean	–	207.12	1.18	11.87	9.05	0.148	1058
std	–	8.85	0.080	0.52	0.63	0.042	12.70

Max–min normalization results for the six metrics are shown in Fig. 27. Compared to the previous 2D case, the correlation between the evaluated metrics and the number of tensile members is more complex, and deviations in the evaluated metrics are larger. For the GS-STM method, as the number of tensile members increases (from 21 to 43), a relatively clear improvement in the GS-STM designs can be observed, resulting in a reduction in strain energy and steel usage, and also an increase in load capacity and material efficiency. However, compared to the GS-STM method, when employing a similar number of tensile members, the material efficiency and constructability indices associated with the C-STM designs are better. For designs C-STM-19a and GS-STM-26, containing 19 and 26 ties respectively, similar material efficiency indices are obtained, though the C-STM-19a design is simpler.

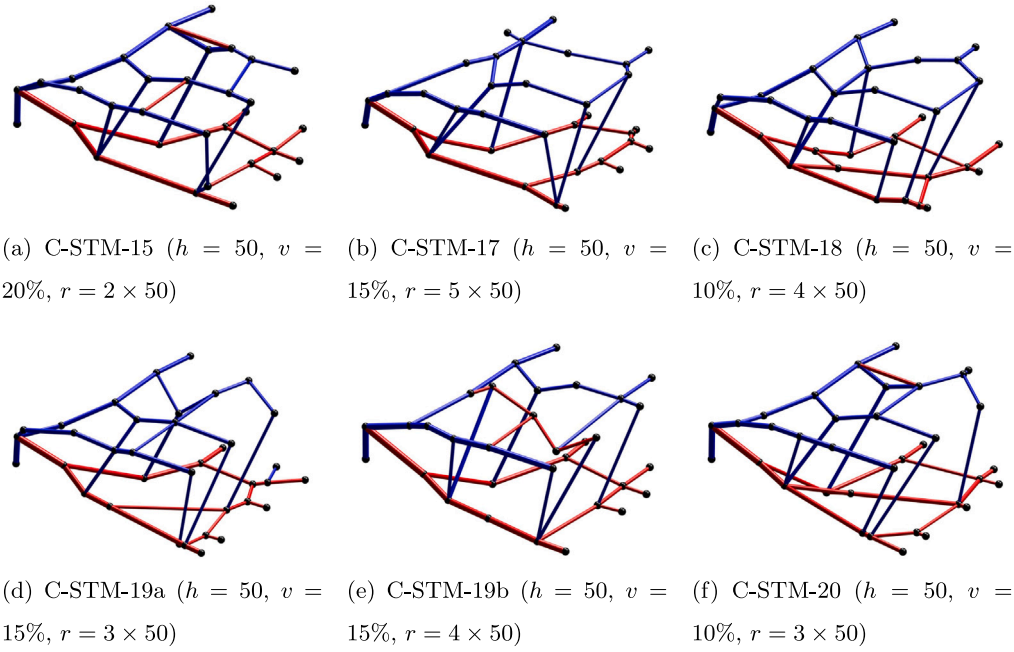

(a) C-STM-15 ($h = 50$, $v = 20\%$, $r = 2 \times 50$) (b) C-STM-17 ($h = 50$, $v = 15\%$, $r = 5 \times 50$) (c) C-STM-18 ($h = 50$, $v = 10\%$, $r = 4 \times 50$)

(d) C-STM-19a ($h = 50$, $v = 15\%$, $r = 3 \times 50$) (e) C-STM-19b ($h = 50$, $v = 15\%$, $r = 4 \times 50$) (f) C-STM-20 ($h = 50$, $v = 10\%$, $r = 3 \times 50$)

Fig. 25. 3D dapped-end voided slab: generated C-STMs with different number of members. The adopted parameters (mesh size, volume fraction and filter radius) in the CSTM method are indicated as h (mm), v and r (mm), respectively.

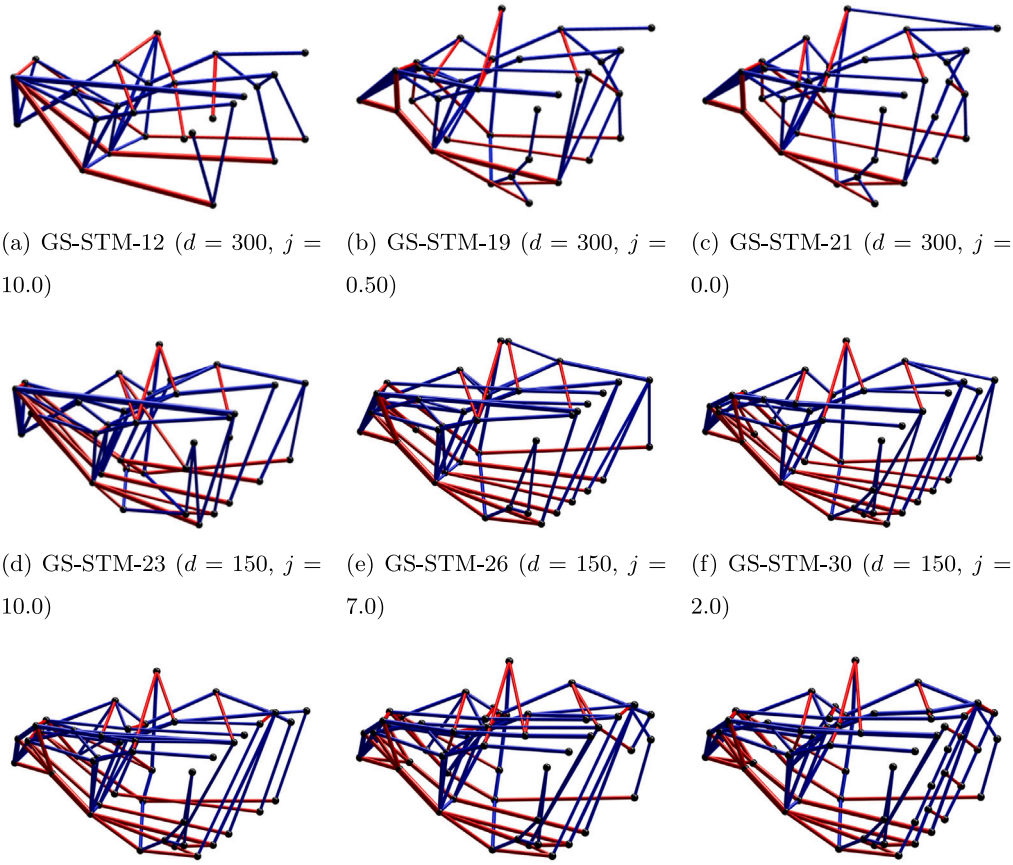

(a) GS-STM-12 ($d = 300$, $j = 10.0$) (b) GS-STM-19 ($d = 300$, $j = 0.50$) (c) GS-STM-21 ($d = 300$, $j = 0.0$)

(d) GS-STM-23 ($d = 150$, $j = 10.0$) (e) GS-STM-26 ($d = 150$, $j = 7.0$) (f) GS-STM-30 ($d = 150$, $j = 2.0$)

(g) GS-STM-35 ($d = 150$, $j = 0.80$) (h) GS-STM-39 ($d = 150$, $j = 0.01$) (i) GS-STM-43 ($d = 150$, $j = 0.0$)

Fig. 26. 3D dapped-end voided slab: generated GS-STMs with different number of members.

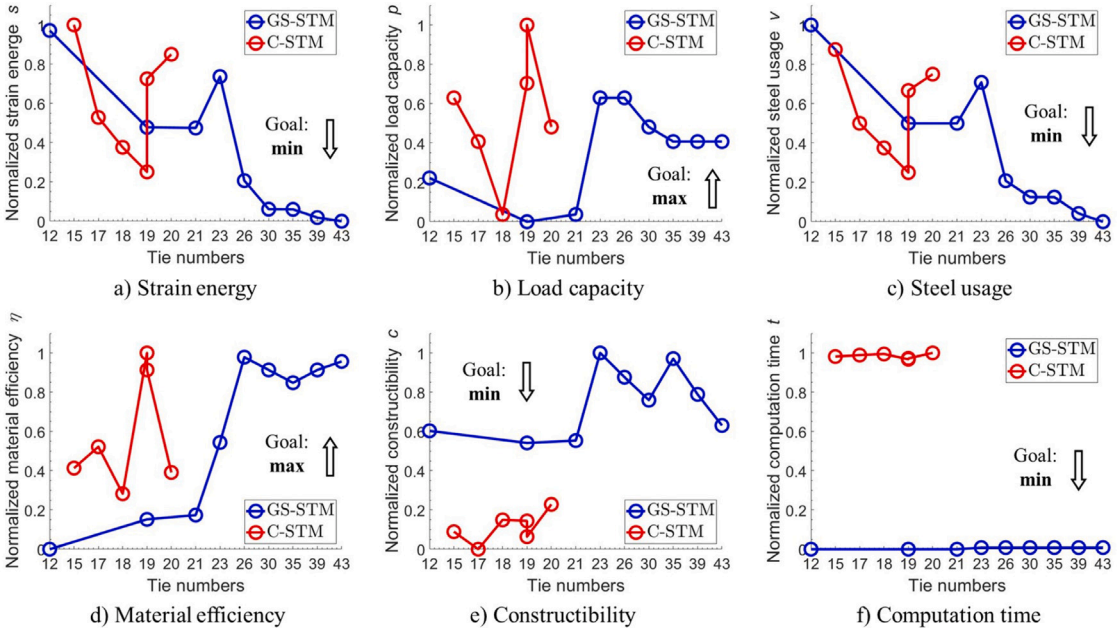

Fig. 27. 3D dapped-end voided slab: max–min normalization of evaluation results for STMs with differing numbers of ties. The arrows in the subfigures indicate the goal of the corresponding metrics.

6. Conclusions

The ground-structure (GS) and continuum (C) based topology optimization approaches are the two main strut-and-tie modelling (STM) methods that can be applied to the conceptual design of reinforced concrete structural elements, here referred to as the GS-STM and C-STM generation methods respectively. Although both methods can be used to generate strut-and-tie (ST) models, their relative performance appears not to have been systematically investigated previously. In the present paper, the GS-STM and C-STM procedures are briefly introduced, with structural performance, economic aspects and method applicability metrics then proposed to facilitate objective evaluation of the performance of the two methods. Specifically, six factors are formulated to quantify these aspects: strain energy of the generated ST models; computational cost; ultimate load capacity of the designed structural element; steel usage; constructability; and material efficiency ratio. A comparison procedure is then proposed to evaluate the generated ST models, enabling their performance to be compared. The two generation methods investigated both start from a topology optimization process, but employ different modelling idealizations; to obtain applicable STM models, additional steps are required in both generation processes. Example problems involving typical D-regions are considered, two 2D cases and one 3D case, with the performance of the corresponding ST designs compared based on the proposed comparison procedure. In addition, the influence of using different input parameters on the efficacy of the two methods is investigated, with the performance of the generated STMs compared.

Based on the example design problems considered, it is found that the STM designs generated using the two methods both lead to safe designs, with the load capacity always larger than the design load. The finite element model used in our publication showed that the optimized designs were always conservative in their load carrying capacity compared to the finite element results, as the analyses showed conservative results ranging from 3% to 30% for the case studies presented with a mean of 17%, where the finite element analysis results themselves can also be assumed conservative, as mentioned previously. Also, the steel usage and material efficiency ratios of the obtained STM designs are found to be comparable. However, the GS-STM method outperforms the C-STM method in terms of computational cost, especially for the 3D case. Considering flexibility in generating STMs with varying numbers of members, it is found that STM designs containing a wide range of numbers of ties can be obtained using the GS-STM method. However, constructability is adversely affected when a large number of tensile members are involved. Overall, both the GS-TO and C-TO methodologies show great potential when seeking efficient ST models in reinforced concrete structures, though are prone to identify designs that are difficult to realize in practice. Considering additional means of quantitatively assessing constructability, and incorporating methods of increasing this in the STM model generation process, is an important future research topic. In addition, considering the use of both experimental testing and numerical simulation to verify STM designs is also an important research topic when considering the applicability of a given STM method.

CRediT authorship contribution statement

Yi Xia: Writing – original draft, Methodology, Investigation, Funding acquisition, Conceptualization. **Andrew Liew:** Writing – review & editing, Writing – original draft, Methodology, Investigation, Funding acquisition, Conceptualization. **Hongfei Wu:** Writing – review & editing. **Matthijs Langelaar:** Writing – review & editing, Supervision, Methodology, Conceptualization. **Max A.N. Hendriks:** Writing – review & editing, Supervision, Methodology, Conceptualization. **Yuanlong Yang:** Writing – review & editing. **Meisam Takalloozadeh:** Writing – review & editing. **Matthew Gilbert:** Writing – review & editing, Methodology, Funding acquisition, Conceptualization.

Declaration of competing interest

The authors declare the following financial interests/personal relationships which may be considered as potential competing interests: Yi Xia reports financial support was provided by National Key Research and Development Program of China. Yi Xia reports financial support was provided by National Natural Science Foundation of China. Yi Xia reports financial support was provided by China Postdoctoral Science Foundation. Matthew Gilbert reports financial support was provided by Engineering and Physical Sciences Research Council. Andrew Liew reports financial support was provided by Engineering and Physical Sciences Research Council. If there are other authors, they declare

that they have no known competing financial interests or personal relationships that could have appeared to influence the work reported in this paper.

Data availability

Data will be made available on request.

Acknowledgements

Yi Xia acknowledges the support of the National Key R&D Program of China (2022YFC3801700), the National Natural Science Foundation of China (52308141) and the China Postdoctoral Science Foundation (2022M720579). Matthew Gilbert and Andrew Liew acknowledge the 'Knowledge Exchange' funding provided by the Engineering and Physical Research Council (EPSRC).

References

[1] Ritter W. Die Bauweise Hennebique. Schweizerische Bauzeitung 1899;33:59–61.
[2] Mörsch E. Concrete-steel construction,(der eisenbetonbau), English Translation of the 3rd German Edition, vol. 33, New York: McGraw-Hill Book Co.; 1909.
[3] Schlaich J, Schafer K, Jennewein M. Toward a consistent design of structural concrete. PCI J 1987;32:74–150. http://dx.doi.org/10.15554/pcij.05011987.74.150,.
[4] Schlaich J, Schafer K. Design and detailing of structural concrete using Strut-and-Tie models. Struct Eng 1991;69:113–25.
[5] Nielsen MP, Hoang LC. Limit analysis and concrete plasticity. CRC Press; 2016.
[6] Yu M, Li J, Ma G. Theorems of limit analysis. Struct Plast: Limit, Shakedown Dyn Plastic Anal Struct 2009;64–73.
[7] El-Metwally S, Chen W-F. Structural concrete: Strut-and-tie models for unified design. CRC Press; 2017.
[8] European Committee for Standardization (CEN). Eurocode 2: Design of concrete structures-Part 1-1: General rules and rules for buildings. 2017.
[9] fib (International Federation for Structural Concrete). fib model code for concrete structures 2010. Lausanne, Switzerland: Ernst & Sohn, Wiley; 2013.
[10] American Concrete Institute (ACI). Building code requirements for structural concrete and commentary. Farmington Hills, MI: ACI Committee 318-14; 2008.
[11] Canadian Standards Association. Design of concrete structures. Rexdale, Ontario: CSA; 2004.
[12] American Association of State Highway Officials and Transportation (AASHTO). LRFD bridge design specifications. 7th ed.. Washington, DC: AASHTO; 2014.
[13] Reineck K-H. Examples for the design of structural concrete with Strut-and-Tie models. American Concrete Institute; 2002.
[14] Chen BS, Hagenberger MJ, Breen JE. Evaluation of Strut-and-Tie modeling applied to dapped beam with opening. ACI Struct J 2002;99:445–50.
[15] Ley MT, Riding KA, Bae S, Breen JE, et al. Experimental verification of Strut-and-Tie model design method. ACI Struct J 2007;104:749–55.
[16] Menichini G, Gusella F, Orlando M. Methods for evaluating the ultimate capacity of existing RC half-joints. Eng Struct 2024;299:117087.
[17] Dorn WS, Gomery R, Greenberg HJ. Automatic design of optimal structures. J Mec 1964;3:25–52.
[18] Biondini F, Bontempi F, Malerba PG. Optimal Strut-and-Tie models in reinforced concrete structures. Comput Assist Mech Eng Sci 1999;6:280–93.
[19] Biondini F, Bontempi F, Malerba PG. Stress path adapting Strut-and-Tie models in cracked and uncracked RC elements. Struct Eng Mech 2001;12:685.
[20] Ali MA, White RN. Formulation of optimal Strut-and-Tie models in design of reinforced concrete structures. ACI Spec Publ 2000;193:979–98.
[21] Ali MA, White RN. Automatic generation of Truss model for optimal design of reinforced concrete structures. ACI Struct J 2001;98:431–42.
[22] Kwak HG, Noh SH. Determination of Strut-and-Tie models using evolutionary structural optimization. Eng Struct 2006;28:1440–9. http://dx.doi.org/10.1016/j.engstruct.2006.01.013.
[23] Zhong JT, Wang L, Deng P, Zhou M. A new evaluation procedure for the Strut-and-Tie models of the disturbed regions of reinforced concrete structures. Eng Struct 2017;148:660–72. http://dx.doi.org/10.1016/j.engstruct.2017.07.012.
[24] Zhong J, Wang L, Zhou M, Li Y. New method for generating Strut-and-Tie models of three-dimensional concrete anchorage zones and box girders. ASCE J Bridge Eng 2017;22(8):04017047. http://dx.doi.org/10.1061/(ASCE)BE.1943-5592.0001078.
[25] Bołbotowski K, Sokół T. New method of generating Strut and Tie models using truss topology optimization. In: Advances in mechanics: theoretical, computational and interdisciplinary issues-3rd Polish congress of mechanics, PCM 2015 and 21st international conference on computer methods in mechanics, CMM. 2015.
[26] Liang QQ, Xie YM, Steven GP. Topology optimization of Strut-and-Tie models in reinforced concrete structures using an evolutionary procedure. ACI Struct J 2000;97:322–32.
[27] Guan H. Strut-and-Tie model of deep beams with web openings-an optimization approach. Struct Eng Mech 2005;19:361–80.
[28] Leu LJ, Huang CW, Chen CS, Liao YP. Strut-and-Tie design methodology for three-dimensional reinforced concrete structures. ASCE J Struct Eng 2006;132:929–38.
[29] Almeida VS, Simonetti HL, Neto LO. Comparative analysis of Strut-and-Tie models using smooth evolutionary structural optimization. Eng Struct 2013;56:1665–75. http://dx.doi.org/10.1016/j.engstruct.2013.07.007.
[30] Bruggi M. Generating Strut-and-Tie patterns for reinforced concrete structures using topology optimization. Comput Struct 2009;87:1483–95. http://dx.doi.org/10.1016/j.compstruc.2009.06.003,.
[31] Bruggi M. On the automatic generation of strut and tie patterns under multiple load cases with application to the aseismic design of concrete structures. Adv Struct Eng 2010;13:1167–81. http://dx.doi.org/10.1260/1369-4332.13.6.1167,.
[32] Bruggi M. A numerical method to generate optimal load paths in plain and reinforced concrete structures. Comput Struct 2016;170:26–36. http://dx.doi.org/10.1016/j.compstruc.2016.03.012.
[33] Jewett JL, Carstensen JV. Topology-optimized design, construction and experimental evaluation of concrete beams. Autom Constr 2019;102:59–67.
[34] Shobeiri V. Determination of Strut-and-Tie models for structural concrete under dynamic loads. Can J Civil Eng 2019;46(12):1090–102. http://dx.doi.org/10.1139/cjce-2018-0780.
[35] Shobeiri V, Ahmadi-Nedushan B. Bi-directional evolutionary structural optimization for Strut-and-Tie modelling of three-dimensional structural concrete. Eng Optim 2017;49:2055–78.
[36] Herranz UP, Maria HS, Gutiérrez S, Riddell R. Optimal Strut-and-Tie models using full homogenization optimization method. ACI Struct J 2012;109:605–14.
[37] Gaynor AT, Guest JK, Moen CD. Reinforced concrete force visualization and design using bilinear truss-continuum topology optimization. ASCE J Struct Eng 2013;139:607–18. http://dx.doi.org/10.1061/(ASCE)ST.1943-541X.0000692.
[38] Jewett JL, Carstensen JV. Experimental investigation of Strut-and-Tie layouts in deep RC beams designed with hybrid bi-linear topology optimization. Eng Struct 2019;197:109322.
[39] He Z-Q, Liu Z, Wang J, Ma ZJ. Development of Strut-and-Tie models using load path in structural concrete. J Struct Eng 2020;146(5):06020004.
[40] El-Zoughiby ME. Z-shaped load path: A unifying approach to developing Strut-and-Tie models. ACI Struct J 2021;118(3):35–48.
[41] Lourenço MS, Fernández Ruiz M, Blaauwendraad J, Bousias S, Hoang LC, Mata-Falcón J, et al. Design and assessment of concrete structures with Strut-and-Tie models and stress fields: From simple calculations to detailed numerical analysis. Struct Concrete 2023;24(3):3760–78.
[42] Xia Y, Langelaar M, Hendriks MAN. A critical evaluation of topology optimization results for Strut-and-Tie modeling of reinforced concrete. Comput-Aided Civ Infrastruct Eng 2020;35(8):850–69. http://dx.doi.org/10.1111/mice.12537.
[43] Xia Y, Langelaar M, Hendriks MAN. Automated optimization-based generation and quantitative evaluation of Strut-and-Tie models. Comput Struct 2020;238:106297. http://dx.doi.org/10.1016/j.compstruc.2020.106297.
[44] Xia Y, Langelaar M, Hendriks MAN. Optimization-based three-dimensional Strut-and-Tie model generation for reinforced concrete. Comput-Aided Civ Infrastruct Eng 2021;36(5):526–43.
[45] He L, Gilbert M. Rationalization of trusses generated via layout optimization. Struct Multidiscip Optim 2015;52:677–94.
[46] Fairclough H, Gilbert M. Layout optimization of simplified trusses using mixed integer linear programming with runtime generation of constraints. Struct Multidiscip Optim 2020;61(5):1977–99.
[47] Fairclough HE, He L, Pritchard TJ, Gilbert M. LayOpt: An educational web-app for truss layout optimization. Struct Multidiscip Optim 2021;64(4):2805–23.
[48] Pressmair N, Xia Y, Wu H. Bridging the gap between mathematical optimization and structural engineering: Design, experiments and numerical simulation of optimized concrete girders. Struct Concrete 2023;24:5314–30. http://dx.doi.org/10.1002/suco.202201096,.
[49] Smith CJ, Gilbert M, Todd I, Derguti F. Application of layout optimization to the design of additively manufactured metallic components. Struct Multidiscip Optim 2016;54:1297–313,.
[50] Xia Y, Langelaar M, Hendriks MA. Optimization-based Strut-and-Tie model generation for reinforced concrete structures under multiple load conditions. Eng Struct 2022;266:114501.
[51] Gilbert M, Tyas A. Layout optimization of large-scale pin-jointed frames. Eng Comput 2003;20(8):1044–64. http://dx.doi.org/10.1108/02644400310503017.
[52] Pritchard T-J, Gilbert M, Tyas A. Plastic layout optimization of large-scale frameworks subject to multiple load cases, member self-weight and with joint length penalties. In: Proceedings of 6th world congress on structural and multidisciplinary optimization. Rio de Janeiro, Brazil; 2005.
[53] Sokół T. A 99 line code for discretized Michell truss optimization written in mathematica. Struct Multidiscip Optim 2011;43(2):181–90. http://dx.doi.org/10.1007/s00158-010-0557-z.

[54] Zegard T, Paulino GH. GRAND—Ground structure based topology optimization for arbitrary 2D domains using MATLAB. Struct Multidiscip Optim 2014;50(5):861–82. http://dx.doi.org/10.1007/s00158-014-1085-z.
[55] Bendsoe MP, Sigmund O. Topology optimization: Theory, methods, and applications. Berlin Heidelberg: Springer Verlag; 2003.
[56] Bendsøe MP, Ben-Tal A, Zowe J. Optimization methods for truss geometry and topology design. Struct Optim 1994;7:141–59.
[57] de Putter A, Hendriks MAN, Rots JG, Yang Y, Engen M, van den Bos AA. Quantification of the resistance modeling uncertainty of 19 alternative 2D nonlinear finite element approaches benchmarked against 101 experiments on reinforced concrete beams. Struct Concrete 2022;23(5):2895–909. http://dx.doi.org/10.1002/suco.202100574.